

# A Hybrid Three-Port Topology for Urban Charging Stations

Mohammadreza Khodaparast Klidbari<sup>1</sup>, Naser Souri<sup>2</sup>, Zahra Sadat Habibolahi<sup>3</sup>, Hamid Montazeri Hedeshi<sup>4</sup>

<sup>1</sup>Faculty of Electrical Engineering, K. N. Toosi University of Technology, Tehran, Iran.

<sup>2</sup>The Bradley Department of Electrical and Computer Engineering, Virginia Tech, United States

<sup>3</sup>Department of Electrical Engineering, Iran University of Science and Technology, Tehran, Iran

<sup>4</sup>Faculty of Electrical and Computer Engineering, University of Tabriz, Tabriz, Iran

Emails: <sup>1</sup>khpmohammadreza@email.kntu.ac.ir, <sup>2</sup>nsouri@vt.edu, <sup>3</sup>zahra\_habibolahi78@elec.iust.ac.ir, <sup>4</sup>h.montazeri.h@gmail.com

**Abstract**—Electric vehicles are rapidly gaining popularity as a sustainable alternative to conventional gasoline. In urban areas, chargers with different ratings can accommodate the diverse needs of electric vehicles. However, the available multiport topologies have variable switching frequencies. This paper introduces a hybrid multiport isolated DC-DC converter for urban charging stations, incorporating fast and slow charging ports with a fixed switching frequency. It provides isolation and enables soft switching on the primary side of the converter without circulating current on its secondary side. The primary side does not need feedback, which reduces complexity. The second stage generates a wide output voltage range to charge the electric vehicle battery by employing a switch. In addition, the proposed topology offers reduced component count and simple control with fixed-frequency operation. This paper provides the concept and the operation modes. Experimental results are provided to validate its features. The prototype converter achieves 96% peak efficiency.

**Index Terms**—DC-DC converters, EV charging station, topology, multi-port converter, ZVS.

## I. INTRODUCTION

Increasing greenhouse gas emissions from the automotive industry is a concerning issue. Electric and hybrid electric vehicles have received significant attention in recent years with advancements in battery technology [1], [2]. Their potential to lower greenhouse gas emissions and lessen reliance on fossil fuels promotes sustainable transportation. Therefore, charging stations are increasing in number in urban areas. Charging stations can benefit from an AC or DC grid. Fig. 1 shows a DC-based charging station structure supplying from both AC and DC sources. DC grids have fewer power conversion stages than AC grids, reducing power conversion losses and potentially increasing efficiency as electric vehicle batteries are also powered with DC [3]–[5].

Slow charging stations, commonly known as level 2, are ideal for overnight charging or suitable for parking periods, while fast charging is ideal for long journeys and rapid energy replenishment in suburban areas, ensuring that drivers can

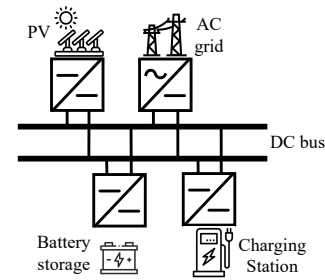


Fig. 1. Charging station topology.

conveniently and efficiently charge their vehicles. Therefore, hybrid charging stations enhance flexibility, accommodating various charging speeds for a diverse range of EVs [6], [7]. Hybrid charging stations can benefit from multiport topologies, as they can integrate fast and slow chargers in one package, as shown in Fig. 2. In addition, multiport topologies usually offer a lower number of components, which reduces the cost.

Among multiport topologies, LLC provides a simple structure with zero-voltage switching (ZVS) capability on its primary side and a wide range of output voltage [8]. ZVS ensures that the voltage across the switch is zero when it turns on or off, reducing the switching losses. The main challenge for LLC topology is that the switching frequency is not fixed and varies according to the output voltage. On the other hand, to achieve a high gain, the switching frequency should be less than the resonant frequency. However, reducing the switching frequency affects the transformer and inductor size. In contrast, considering a higher switching frequency increases the switching losses. In addition, adjusting the voltage gain using the switching frequency complicates the transformer design and can lead to a reduction in efficiency [9], [10].

For EV applications, it is recommended that the input and output are galvanically isolated so that battery protection is not affected by the charging system. However, [11], [12] propose topologies that isolation is not respected. References [7], [13], [14] present an isolated three-port topology with two LLC resonant tanks that can operate at a high switching frequency with lower switching losses due to soft-switching operation. However, the design of these topologies is complex

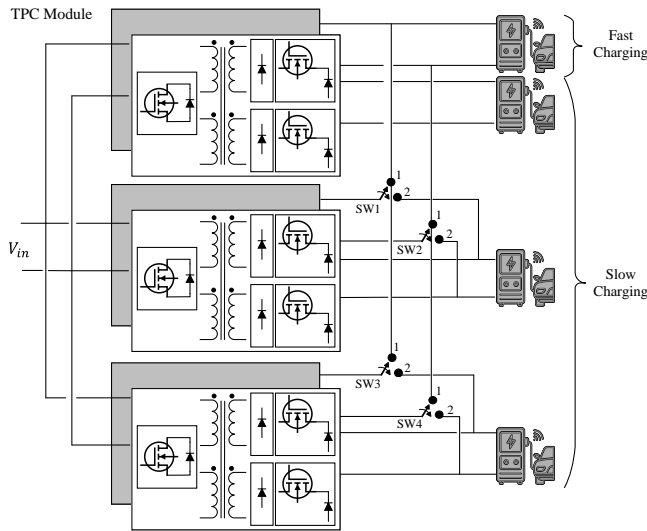


Fig. 2. A hybrid charging station block diagram.

as they use a three-winding transformer. In addition, this type of transformer introduces a circulating current, which increases the losses and stress over the components. Therefore, an additional control algorithm is required to minimize this current. Reference [15] proposes a topology that the frequency is fixed during some modes. However, it changes in other modes. Therefore, [16] proposes a new topology that uses a fixed frequency. However, this topology has a single port structure. Moreover, it has a large number of components, which increases the cost. To overcome the existing drawbacks, a new multiport SiC-based isolated topology is proposed in this paper to address the aforementioned issues. Table I shows a comparison of different topologies. This comparison is based on the control method, the number of ports, the circulating current, the number of components, and the bidirectional or unidirectional structure.

The contribution of this paper is as follows.

- Proposing a new single-stage multiport topology for hybrid charging stations with fixed frequency.

Section II provides the proposed topology, its features, and its operation modes. Section III provides simulation studies to evaluate the switching waveforms. Section IV provides experimental studies to validate the effectiveness of the proposed topology. In the last section, a conclusion is provided.

## II. PROPOSED MULTI-PORT TOPOLOGY

This section studies the concept of the proposed charger topology and the operating modes. Fig. 3 shows the proposed LLC topology for a charging station. This topology consists of two stages and two outputs, one of which is fast charging, and the other is slow charging. The primary side of this converter is a full bridge converter, and the switching frequency is close to the resonance frequency. The transformer isolates the primary and secondary sides. The power is shared between the secondary sides through this transformer. ZVS occurs for the primary switches, reducing the switching losses. However, the charging algorithm is implemented on the secondary side. The

proposed topology utilizes a two-winding transformer instead of a three-winding transformer, resulting in eliminating the circulating current and reducing complexity. To achieve ZVS during dead time, the magnetizing current of the transformer  $I_m$  must be capable of charging and discharging the capacitors  $C_{oss}$ . The current that passes through each of the output capacitors  $C_{oss}$  is calculated as follows.

$$I_{coss} = C_{oss} \frac{\Delta V}{\Delta t} \quad (1)$$

where  $I_{coss} = (I_{lm1} + I_{lm2})/2$  and  $I_{lm1,2} = V_{out1,2}/4L_m f_s$ , and  $f_s$  is the switching frequency. Therefore, the duration for charging the capacitor  $C_{oss}$  should be less than the dead time to achieve zero-voltage switching. Fig.4 shows the circuit in different operation modes for the proposed topology. These modes are discussed below.

### A. Operation Mode I: $t_1 \leq t < t_2$

Fig. 4(a) shows the equivalent circuit in this operation mode during  $t_1$  to  $t_2$ . In this mode,  $S_2$  and  $S_3$  are ON at the primary side. At the beginning of this interval, the voltage across the MOSFET is zero as the body diode conducts before  $t_1$ , which indicates a ZVS. In this mode,  $I_{lr1}$  and  $I_{lr2}$  are positive and greater than  $I_{lm1}$  and  $I_{lm2}$ . As a result, diodes  $D_1, D_4, D_5, D_8$  are ON and  $V_{lm1}$  and  $V_{lm2}$  are equal to  $V_{o1}$  and  $V_{o2}$ , respectively.

### B. Operation Mode II: $t_2 \leq t < t_3$

In this mode,  $S_2$  and  $S_3$  are ON and  $S_1$  and  $S_4$  are OFF as shown in Fig. 4(b). In this mode,  $I_{lr2}$  reaches  $I_{lm2}$  at  $t_2$ , and the secondary side of  $T_2$  is zero. In this case, the magnetizing inductor at the primary side of this transformer resonates with the resonant tank, which is calculated from  $f_{sr2} = \frac{1}{2\pi\sqrt{(l_r + l_m)c_r}}$ .

### C. Operation Mode III: $t_3 \leq t < t_4$

In this mode, all switches are OFF, as shown in Fig. 4(c).  $I_{lr1}$  is greater than  $I_{lm1}$  in this mode, helping  $I_{lm1}$  to charge and discharge the capacitors  $C_{oss}$  to achieve ZVS. The resonant tank current passes through the output capacitor of the switches, and based on the current direction, it charges the capacitor of the switches  $S_2$  and  $S_3$ , and discharges  $S_1$  and  $S_4$ . Finally, the capacitors  $C_{oss}$  are fully charged and discharged, and the current passes through the body diodes  $S_{1,4}$ .

### D. Operation Mode IV: $t_4 \leq t < t_5$

In this mode, the body diodes of  $S_1$  and  $S_4$  are ON, and  $D_1$  and  $D_2$  conduct as shown in Fig. 4(d). The direction of the inductors current remains unchanged during this interval. In addition,  $I_{lr1}$  and  $I_{lr2}$  pass through the body diodes of  $S_1$  and  $S_4$ . The  $V_{DS}$  is, therefore, zero for  $S_1$  and  $S_4$ .

### E. Operation Mode V: $t_5 \leq t < t_6$

In this mode,  $S_1$  and  $S_4$  are ON and  $D_2, D_3, D_6,$  and  $D_7$  conduct as shown in Fig. 4(e). In the previous mode (IV), the body diodes of  $S_1$  and  $S_4$  are ON. Therefore, the corresponding switches turn on with ZVS.

Fig. 5. shows the current and voltage waveforms of the diodes, switches, and the magnetizing current during the

TABLE I  
COMPARISON OF DIFFERENT TOPOLOGIES.

Reference	Control method	Circulating current	Port	Switching	Direction	Transformers	Inductors	Diodes	Switches
Proposed	Fixed $F_{sw}$ , PWM	No	Multiport	ZVS	Unidirectional	2	4	8	6
[16]	Variable $F_{sw}$ , PWM	No	Single port	ZVS	Unidirectional	3	3	8	6
[17]	Variable $F_{sw}$ , PSH	Yes	Multiport	ZVS	Unidirectional	2	2	4	6
[18]	Variable $F_{sw}$ , PWM	Yes	Multiport	ZVS	Unidirectional	1	2	8	8
[19]	Fixed $F_{sw}$ , PS-PWM	Yes	Multiport	Hard	Unidirectional	1	1	8	8
[20]	Variable $F_{sw}$ , PSH	No	Multiport	ZVS	Unidirectional	1	2	0	12

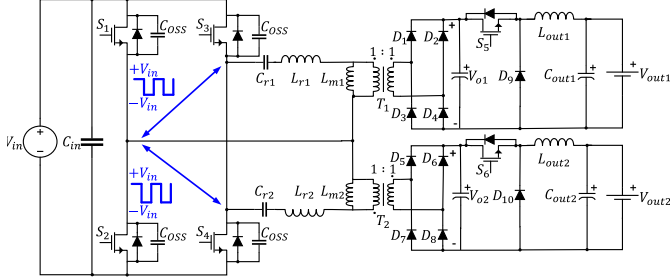


Fig. 3. Proposed multiport LLC topology for a hybrid charging station.

operation modes.  $G_1$ ,  $G_4$ ,  $V_{s3}$ , and  $V_{s4}$  are the gate drive commands and the switch voltages for  $S_1$  and  $S_4$  from the top, respectively. In this figure,  $I_{Lm1}$ ,  $I_{Lm2}$ ,  $I_{Lr1}$ , and  $I_{Lr2}$  are the magnetizing current and inductor current for the transformers, respectively. During the charging interval,  $I_{D1}$ ,  $I_{D3}$ ,  $I_{D5}$ , and  $I_{D7}$  show the output rectifier currents, respectively.

#### F. Resonant Tank Design

This section discusses the designs of  $L_r$  and  $C_r$ . The transformer leakage inductor  $L_r$  affects the resonant tank gain and the resonance frequency. To reduce the effect of leakage inductance on the resonance frequency,  $L_r$  should be large enough. The capacitor value is designed based on the resonance frequency and the maximum voltage stress across the capacitor in the resonant tank, which is calculated from:

$$V_{cr}^{\max} = I_{pri}^{\text{peak}} \sqrt{\frac{L_r}{C_r}} \quad (2)$$

where  $I_{pri}^{\text{peak}}$  is the primary peak current. The resonance frequency is calculated using  $F_{r1,2} = 1/(2\pi\sqrt{L_r L_c})$ . In practice, the resonant component values may not be equal for both transformers.

### III. SIMULATION RESULTS

Simulation studies are performed in Plexim software to see the switches waveform and the zero-voltage switching operation under different rating power. In the simulation study, both slow and fast chargers are working simultaneously. The simulation tests are done according to Fig. 2, which shows one input and multiple outputs. For simplicity, only one of the parallel converters is included in the simulation studies.

In this simulation study, one of the ports is examined under different rating powers to see the currents and voltages under

TABLE II  
SYSTEM PARAMETERS.

Parameter	Value	Parameter	Value
Input voltage	$V_{in}$ 150 V	Output voltage	$V_O$ 30-137 V
Magnetizing inductance	$L_{m1,2}$ 240 uH	Resonant Inductor	$L_{r1,2}$ 31 uH
Resonant capacitor	$C_{r1,2}$ 60 nF	Resonant frequency	$F_r$ 116 kHz

ZVS. This study assumes that the first port provides power to the load and the second port is deactivated. In these cases, the converter delivers 9 kW, 18 kW, and 26 kW to validate under different ratings. The voltages and currents under these three rating powers are 303 V, 30 A, 425 V, 42.5 A, 510 V, and 51 A, respectively. The simulation results for these case studies are shown in Fig. 6. In this figure,  $I_{s3}$  and  $V_{s3}$  are the current and voltage for one switch of the primary side, and  $V_{o1}$  is the output voltage of the rectified voltage on the secondary side. As shown in this figure, in all cases the proposed topology delivers power under zero-voltage switching.

### IV. EXPERIMENTAL RESULTS

A prototype is built in the lab to evaluate the proposed converter practically. The specification of the converter is shown in Table II. Fig. 7 shows the experimental setup. Two case studies are provided to show the converter efficiency and waveforms, as below.

#### A. Case I: $P_{out1} = 460 \text{ W}$ and $P_{out2} = 80 \text{ W}$

In this case, the converter is examined to see the waveform and validate ZVS. The output power of the first port is assumed to deliver 460 W power to the load, and the second port provides 80 W to the load. In this test, the gate-source and gate driver voltages are captured. The result is shown in Fig. 8(a). As can be seen, the switches achieve zero-voltage switching. In this case study, the converter achieves 96% efficiency.

#### B. Case II: $P_{out1} = 80 \text{ W}$ and $P_{out2} = 450 \text{ W}$

In this case, the converter is examined at another rating power. The output power of the first port is assumed to provide 80 W power to the load, and the second port delivers 450 W to the load in the case. In this test, the gate-source and gate driver voltages are captured. The result is shown in Fig. 8(b). As can be seen, the switches achieve zero-voltage switching.

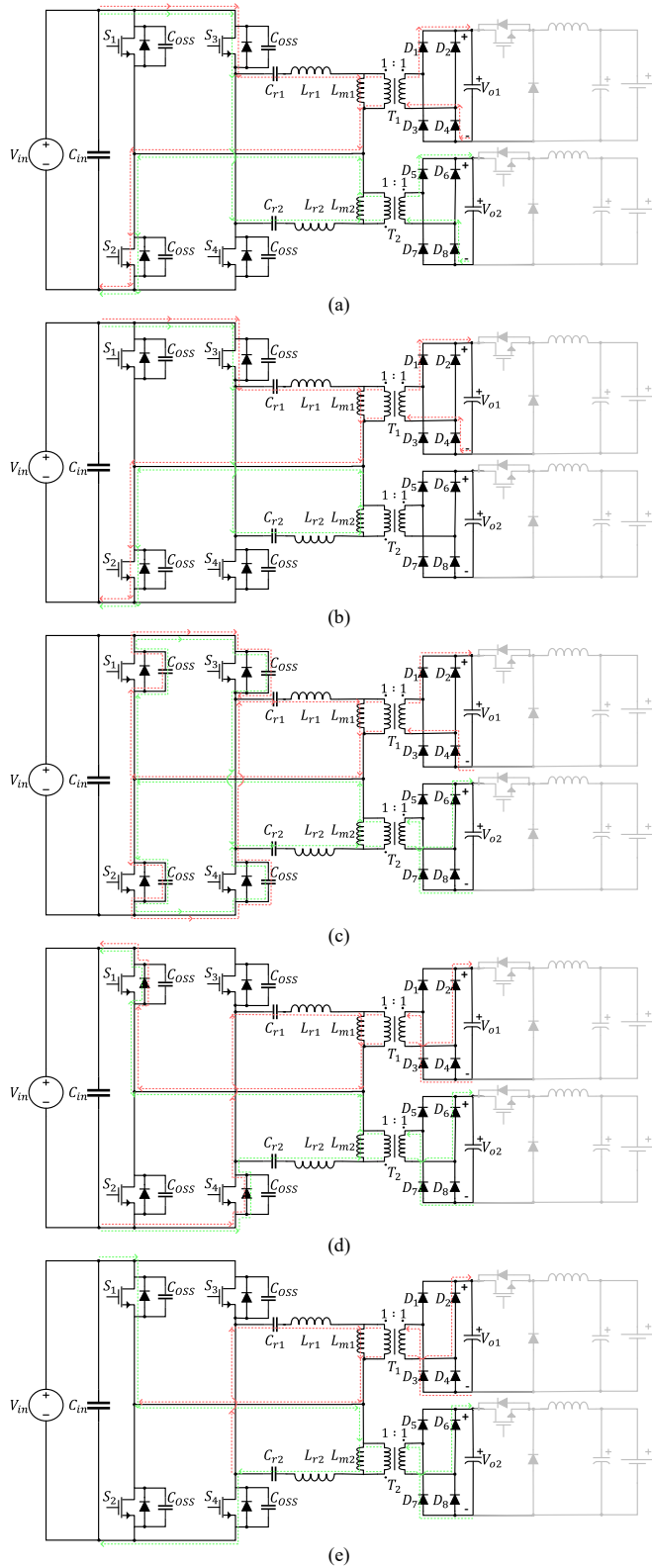


Fig. 4. Operation modes of the topology: (a) mode I, (b) mode II, (c) mode III, (d) mode IV, (e) mode V.

In this case study, the converter achieves 96% efficiency using SiC-based switches.

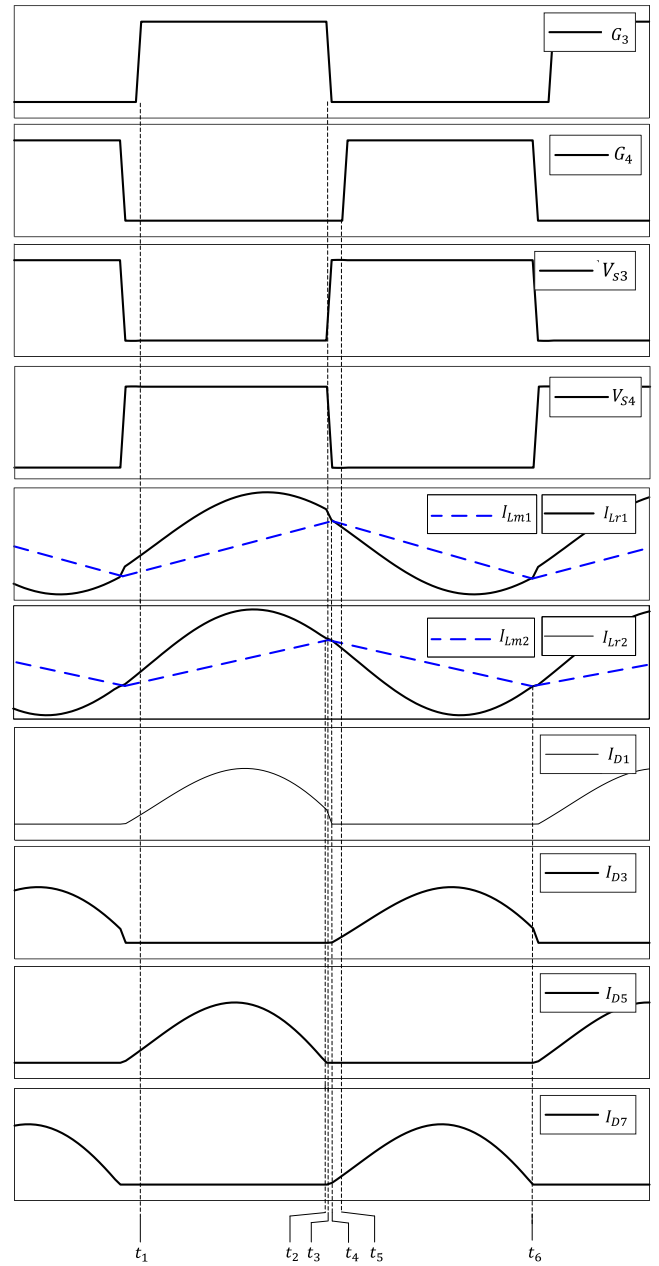


Fig. 5. Voltages and currents of the switches and diodes in steady-state operation.

## V. CONCLUSION

This paper proposes a hybrid three-port isolated DC-DC converter, which is based on the LLC resonant topology. This topology is designed specifically for hybrid EV charging stations. The proposed converter features both fast and slow charging ports. The topology uses an LLC resonant tank, providing isolation and enabling soft switching. By eliminating the need for the primary-side feedback signals, the complexity of the control circuit is significantly reduced. The proposed converter offers a lower number of components, which reduces the cost. In addition, it offers a simple control under fixed-frequency operation and ZVS. The efficacy of the converter is demonstrated through a 600 W prototype, validating the operation and its potential benefits for urban EV charging

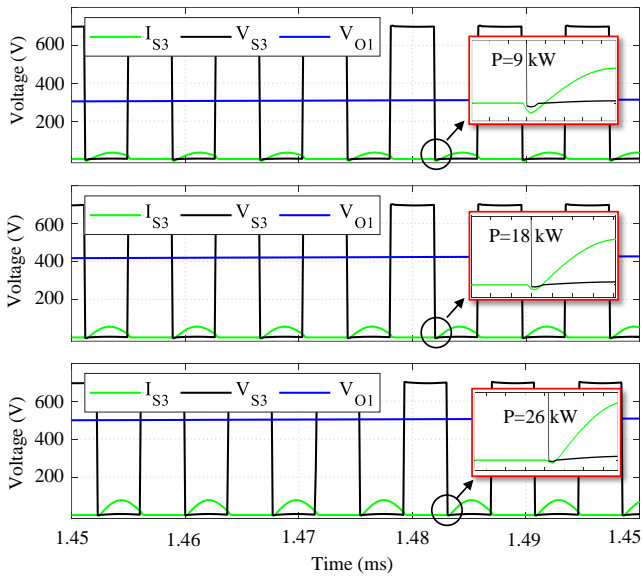


Fig. 6. Voltages and current of a switch at different rating power.

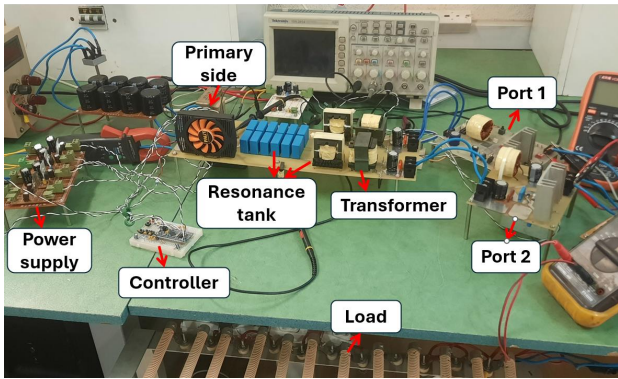


Fig. 7. Experimental setup.

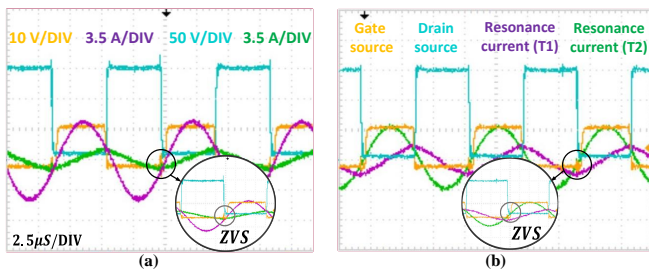


Fig. 8. Experimental results: (a) results for  $P_{out1} = 460$  W and  $P_{out2} = 80$  W, (b) results for  $P_{out1} = 80$  W and  $P_{out2} = 450$  W.

infrastructure. The converter achieves 96% efficiency.

#### ACKNOWLEDGMENT

The authors would like to thank Kv Material, s.r.o company, for the financial support at the conference.

#### REFERENCES

[1] J. Chevinly, S. S. Rad, E. Nadi, B. Proca, J. Wolgemuth, A. Calabro, H. Zhang, and F. Lu, "Gallium nitride (GaN) based high-power multi-level H-bridge inverter for wireless power transfer of electric vehicles," in *IEEE Transportation Electrification Conference and Expo (ITEC)*, Chicago, IL, June 2024.

[2] S. H. Nazaralizadeh, A. Banerjee, P. Srivastava, and Famouri, "Battery

energy storage systems: A review of energy management systems and health metrics," *Energies*, vol. 17, no. 5, p. 1250, March 2024.

[3] N. Souiri and A. Mehrizi-Sani, "Accurate current sharing in a DC micro-grid using modified droop control algorithm," in *Industrial Electronics Society (IES)*, Chicago, IL, June 2024.

[4] M. Ghavaminejad, E. Afjei, and M. Meghdadi, "Double-input/double-output buck-zeta converter," in *29th Iranian Conference on Electrical Engineering (ICEE)*, Tehran, Iran, May 2021.

[5] M. Ghasemi, A. Honarbakhsh, M. Saradarzadeh, and M. Hamzeh, "Ultra-wide voltage range control of DC-DC full-bridge converter with hysteresis controller," in *13th Power Electronics, Drive Systems, and Technologies Conference (PEDSTC)*, February 2022.

[6] S. A. Assadi, Z. Gong, N. Coelho, M. S. Zaman, and O. Trescases, "Modular multiport electric-vehicle DC fast-charge station assisted by a dynamically reconfigurable stationary battery," *IEEE Transactions on Power Electronics*, vol. 38, no. 5, pp. 6212–6223, January 2023.

[7] H. Krishnaswami and N. Mohan, "Three-port series-resonant DC-DC converter to interface renewable energy sources with bidirectional load and energy storage ports," *IEEE Transactions on Power Electronics*, vol. 24, no. 10, pp. 2289–2297, August 2009.

[8] I. Kougioulis, A. Pal, P. Wheeler, and M. R. Ahmed, "An isolated multiport DC-DC converter for integrated electric vehicle on-board charger," *IEEE Journal of Emerging and Selected Topics in Power Electronics*, vol. 11, no. 4, pp. 4178–4198, May 2023.

[9] N. D. Dao, D.-C. Lee, and Q. D. Phan, "High-efficiency SiC-based isolated three-port DC-DC converters for hybrid charging stations," *IEEE Transactions on Power Electronics*, vol. 35, no. 10, pp. 10455–10465, February 2020.

[10] M. Mohebifar, N. Rostami, E. Babaei, and M. Sabahi, "Dual-output step-down soft switching current-fed full-bridge DC-DC converter," in *14th International Conference on Electrical Engineering/Electronics, Computer, Telecommunications and Information Technology (ECTI-CON)*, Phuket, Thailand, June 2017.

[11] J. Y. Yong, V. K. Ramachandaramurthy, K. M. Tan, and J. Selvaraj, "Experimental validation of a three-phase off-board electric vehicle charger with new power grid voltage control," *IEEE Transactions on Smart Grid*, vol. 9, no. 4, pp. 2703–2713, October 2018.

[12] N. Kumar, S. K. Mazumder, and A. Gupta, "SiC DC fast charger control for electric vehicles," in *IEEE Energy Conversion Congress and Exposition (ECCE)*, Portland, OR, December 2018.

[13] Y. Wang, F. Han, L. Yang, R. Xu, and R. Liu, "A three-port bidirectional multi-element resonant converter with decoupled power flow management for hybrid energy storage systems," *IEEE Access*, vol. 6, pp. 61 331–61 341, September 2018.

[14] M. Phattanasak, R. Gavagsaz-Ghoachani, J.-P. Martin, B. Nahid-Mobarakeh, S. Pierfederici, and B. Davat, "Control of a hybrid energy source comprising a fuel cell and two storage devices using isolated three-port bidirectional DC-DC converters," in *Eighth International Conference and Exhibition on Ecological Vehicles and Renewable Energies (EVER)*, May 2013.

[15] Z. Shi, Y. Tang, Y. Zhang, Y. Guo, H. Sun, and L. Jiang, "A secondary-side semiactive 3-phase interleaved resonant converter employing multimode modulation scheme for fast EV charger applications," *IEEE Transactions on Power Electronics*, vol. 37, no. 11, pp. 13 385–13 397, June 2022.

[16] F. Liu, Y. Chen, and X. Chen, "Comprehensive analysis of three-phase three-level LC-type resonant DC-DC converter with variable frequency control—series resonant converter," *IEEE Transactions on Power Electronics*, vol. 32, no. 7, pp. 5122–5131, September 2017.

[17] X. Gao, H. Wu, and Y. Xing, "A multioutput llc resonant converter with semi-active rectifiers," *IEEE Journal of Emerging and Selected Topics in Power Electronics*, vol. 5, no. 4, pp. 1819–1827, June 2017.

[18] Y. Shi and X. Yang, "Wide load range ZVS three-level DC-DC converter: Four primary switches, capacitor clamped, two secondary switches, and smaller output filter volume," *IEEE Transactions on Power Electronics*, vol. 31, no. 5, pp. 3431–3443, August 2016.

[19] S. Rivera, F. Flores-Bahamonde, H. Renaudineau, T. Dragicevic, and S. Kouro, "A buck-boost series partial power converter using a three-port structure for electric vehicle charging stations," in *IEEE 12th Energy Conversion Congress and Exposition - Asia (ECCE-Asia)*, July 2021.

[20] S. S. Chakraborty, S. Dey, and K. Hatua, "Design of a three-winding transformer for power decoupling of a three-port series resonant converter for an integrated on-board EV charger," *IEEE Transactions on Power Electronics*, vol. 38, no. 11, pp. 14 262–14 273, August 2023.